Examination of the Effect of Common CATR Quiet Zone Specifications on Antenna Pattern Measurement Uncertainties

S.F. Gregson*, C.G. Parini†

**NSI-MI Technologies LLC. USA, sgregson@nsi-mi.com,*
†Queen Mary University of London UK, c.g.parini@qmul.ac.uk

Keywords: CATR, Quiet Zone, Performance Specification.

Abstract

The use of uniformity of the quiet-zone (QZ) in determining the maximum size of test antenna that can be measured in a given point-source compact antenna test range (CATR) has been the accepted method since its inception [1]. Furthermore, the definition of a quiet zone (QZ) having amplitude taper of less than 1 dB, amplitude ripple of less than ±0.5 dB in amplitude and ±5° in phase has become a near universal standard both in academia and industry [1]. However, this almost omnipresent usage belies the fact that surprisingly few workers are familiar with what this implies for an actual antenna pattern measurement. The recent development of a novel computational electromagnetic (CEM) simulation tool that permits the simulation of "measured" far-field pattern data for a known CATR and test antenna combination [2] permits the careful examination of the behaviour of these three conventional CATR QZ specifications on "measured" far-field patterns for a given test antenna. Results are presented and discussed.

1 Introduction

The point source compact antenna test range (CATR) uses a parabolic reflector to project an image of the feed antenna at infinity which has the effect of transforming the quasi-spherical wave that is radiated by the feed (which is located at the focal point of the reflector) into a pseudo plane wave which is used to illuminate the test antenna thereby synthesising the classical far-field measurement configuration, only at a greatly reduced physical distance than would otherwise be the case. The criteria for specifying the quality of this pseudo plane wave which is commonly used is: 1 dB amplitude taper, ±0.5 dB amplitude ripple and ±5° phase ripple [1]. The amplitude taper is measured as the variation of a 2nd degree polynomial function that is obtained by means of, typically, a least squares best fit through the amplitude data over a cut through the quiet zone with the value being reported in dB. The amplitude ripple is measured by determining the variation of the amplitude about the 2nd degree polynomial fit with this also being expressed in dB. The phase ripple is characterized by the deviation from a best-fit straight line over the quiet zone and is expressed in degrees. These linear cuts are typically acquired across horizontal, vertical or inter-cardinal cuts that are transverse to the z-axis of the range and are repeated at various z positions down range. The maximum dimensions within a volume of space, typically cylindrical in shape, throughout which this specification can be achieved determines the size of the CATR quiet-zone (QZ) [1]. Amplitude taper and amplitude ripple parameters are illustrated in Figure 1 with the phase ripple being analogous to the amplitude ripple shown (without a taper). These field properties are generally characterised as part of the CATR range installation using a procedure based upon a field probe scanner comprising a probe antenna mounted on a linear translation axis [1, 3]. The final facility acceptance is typically predicated upon the vendor being able to successfully demonstrate that these requirements have been met or exceeded.

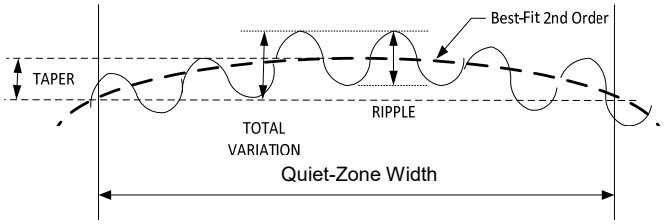

Figure 1: Illustration of CATR amplitude taper and amplitude ripple specifications in the QZ.

Unfortunately, in many cases it is not directly apparent how a given CATR QZ performance specification, when expressed in terms of amplitude taper, amplitude ripple and phase ripple will manifest itself on the resulting far-field antenna pattern measurement.

Previous work in this area is relatively limited. In the early days of CATR development the specification of QZ field amplitude taper of 1 dB and ripple as being less than ±0.5 dB in amplitude and ±5° in phase was determined from a heuristic viewpoint. This is illustrated by [4] through taking scans of QZ amplitude and phase ripple and demonstrating that antennas measured in such QZ where comparable to outdoor far field measurements. Later, computational techniques began to be used and in [5, 6] coupling between the AUT and CATR is expressed in terms of CATR modelling using Geometrical Optics (GO) and Geometric Theory of Diffraction (GTD) and plane wave spectra coupling to the AUT. This work was used to illustrate the design of a CATR in terms of its reflector edge illumination and edge treatment.

With this limited quantification of this well used QZ specification, a sophisticated CEM modelling tool was recently developed [3] that allowed "measured" far-field patterns to be produced for a known CATR-AUT combination with the analysis being based on a well-known reaction theorem [1, 2]. While much of the existing work centred about obtaining the measurement uncertainty for a given CATR and AUT, this paper is primarily concerned with examining the impact that varying the aforementioned specifications has on the resulting antenna measurement and thereby examining and verifying the specification rules.

The following sections examine each of the three specifications in turn so as to be able to establish the behaviour of the measurement artefacts before combining them to obtain the upper bound measurement uncertainty using the concept of an error to signal ratio, which is introduced in the following section.

2 Assessment of Simulation Results

When evaluating antenna test range assessments, the usual method for determining errors through measurement is to isolate and vary a single parameter of the test and observe pattern changes. The change in the measurement parameter is designed to focus on a single error source within the facility level uncertainty budget, such as scattering or receiver linearity. Differences in pattern characteristics, *i.e.* gain, side lobe level, cross-pol level, and pointing are then recorded. Often, it is possible to quantify local pattern differences by computing a signal-to-error level. This signal-to-error ratio can then be used to evaluate the effects of the same error at a different pattern level, [1, 7]. This is a very powerful technique as it permits a generalisation to be made. The error to signal ratio, E/S, can be calculated from the upper bound uncertainty using,

$$E/S\big|_{dB} = 20\log_{10}\left(10^{\frac{\text{Upper Bound Uncertainty}\big|_{dB}}{20}} - 1\right) \qquad (1)$$

Conversely, the upper bound uncertainty can be computed from the error to signal ratio using,

$$\text{Upper Bound Uncertainty}\big|_{dB} = 20\log_{10}\left(1 + 10^{\frac{E/S\big|_{dB}}{20}}\right) \qquad (2)$$

$$\text{Lower Bound Uncertainty}\big|_{dB} = 20\log_{10}\left(1 - 10^{\frac{E/S\big|_{dB}}{20}}\right) \qquad (3)$$

By way of an illustration of this process let us take the example of the upper bound uncertainty at the -25 dB side-lobe level (SLL). Using equation (1) we can show that, an upper bound uncertainty of, say, 0.0983 dB at 0 dB equates to an Error to Signal (E/S) level of -38.876 dB relative to 0 dB. Clearly, relative to a -25 dB side-lobe, this equates to an E/S level of -13.876 dB. Using equation (2) we can see that this corresponds to a 1.601 dB uncertainty at the -25 dB SLL. In this way we can compute the uncertainty at for any desired side lobe level irrespective of whether that side-lobe level exists within the measured pattern. From an examination of equations (2) and (3) it is clear that when the S/E is high (>25 dB), the difference between the lower and upper bounds becomes negligible. However, as the S/E reduces the difference becomes significant. Which one should be chosen is generally a matter of how it will be applied to the final measurement. The measurement uncertainty means that the true value falls somewhere between the upper and lower bounds plus the measurement.

In the example illustrated above, the Equivalent Stray Signal (ESS) ratio is used to estimate the uncertainty in the side-lobe pattern results and represents the magnitude, relative to the peak of the main beam, of an error signal that is associated with the multiple reflection error term. Since side-lobe uncertainties are desired for the full angular range and for different side-lobe levels, it is useful to determine a single value for the ESS/SIG that can be applied to all side-lobes. The peak value could be used, but it could also result in an unreasonably high estimate for most side-lobes. A more reasonable estimate, that also provides a means to assign a confidence level to the uncertainty, is the Root Mean Square (RMS) of the E/S using all the points in the pattern. This has the inherent advantage of increasing the number of points for which the comparison is performed thereby yielding a non-local measure of adjacency.

2 CEM Model

As noted above and developed in [2], the coupling of the pseudo plane-wave into the aperture of an AUT creates the classical measured "far-field" radiation pattern. Assuming the electric and magnetic fields radiated by a given antenna over the convenient enclosing surface are known then, it is possible to create a perfect plane wave and to use that to tap off the far-field pattern at a specific far-field direction be evaluating the reaction integral between the plane wave and the AUT. The electric and magnetic fields of a perfect *x*-polarised plane wave propagating in the positive *z*-direction can be expressed as,

$$\underline{E}(x,y,z) = A(x,y)e^{-jk_0 z}\,\underline{\hat{e}}_x \qquad (4)$$

Here, we have assumed a positive, supressed, time dependency, A is the complex wave amplitude and k_0 is the free-space propagation constant. The corresponding magnetic fields can be obtained from the TEM condition specifically,

$$\underline{H}(x,y,z) = \frac{1}{Z_0}\underline{\hat{u}} \times \underline{E}(x,y,z) \qquad (5)$$

Here, Z_0 is the characteristic impedance of free space. Thus, with the use of equations (4) and (5) we can create a plane wave with amplitude taper, amplitude ripple and phase ripple of our choosing using the definitions set out above. For the simulations presented below, the case of a simulated WR90 pyramidal horn AUT was utilised. Here, the pyramidal horn had an aperture dimension of width 0.144 m, and height 0.194 m with a horn length of 0.378 m, that is excited by the fundamental TE_{10} mode and radiating at 8 GHz. The near electric and magnetic fields were computed across the surface

of an enclosing integrating surface of radius 0.91 m (3'). In the sections that follow, the properties of $A(x, y)$ are specified in terms of the CATR QZ performance parameters defined above across a 1.83 m (6') diameter cylindrical QZ that corresponded to the spherical integrating surface. The following sections examine each of these CATR QZ parameters individually and in each case observe the effect that a variation has on the corresponding "measured" antenna pattern.

2.1 Amplitude Taper

Figure 2 below contains a great circle azimuth far-field pattern cut of the simulated pyramidal horn antenna. The red trace shows the equivalent simulated "measured" far-field cut for the case where the illuminating plane wave had an amplitude taper of 0.25 dB. Here, the amplitude ripple was 0 dB and the phase ripple was 0°. The AUT was offset from the origin of the measurement coordinate system by 0.6096 m thereby insuring that the AUT traversed much of the assumed CATR QZ region. For this case the ratio of the maximum radial extent of the AUT to the CATR QZ was 75.3%. The impact of increasing or decreasing the utilisation of a CATR QZ is examined in a subsequent section. The agreement between the truth model supplied by the ideal far-field pattern and the simulated measurement is very encouraging. The difference level, denoted by the magenta trace, was computed and is not shown as it was below the -60 dB vertical lower limit of the plot. The RMS difference level was computed over the entire great circle cut (and not just across the angular region shown in Figure 2) and was found to be -74.75 dB. Figure 3, 4 and 5 respectively present equivalent results for the case of a 0.5, 1.0 and 1.5 dB amplitude taper with the RMS difference levels being -68.64, -62.76 and -59.28 dB.

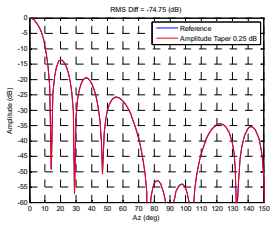

Figure 2: 0.25 dB Amplitude taper across QZ.

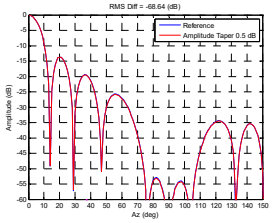

Figure 3: 0.5 dB Amplitude taper across QZ.

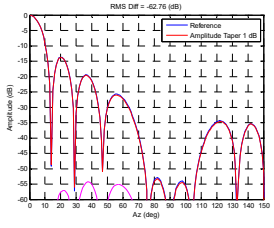

Figure 4: 1.0 dB Amplitude taper across QZ.

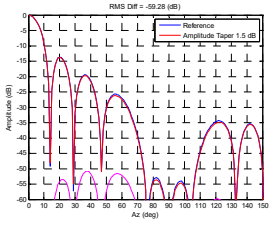

Figure 5: 1.5 dB Amplitude taper across QZ.

This is a very encouraging result as it is clear that even for the case of a 1.5 dB taper, which is significantly greater than the accepted upper bound for this parameter, the RMS difference level was well below many of the other typically observed terms within the range uncertainty budget. Furthermore, the differences were mostly evident in the wide-out pattern and back-lobes which can be a region of lesser interest in many commonly encountered applications.

2.2 Amplitude Ripple

The next parameter that was investigated was amplitude ripple for which the amplitude taper and phase ripple were set to zero. As before, the AUT was offset from the origin of the measurement coordinate system by 0.6096 m. Figures 6, 7, 8 and 9 contain simulations of far-field "measurements". In addition to the amplitude of the ripple the spatial frequency of the ripple must be taken into account and this is examined specifically in Section 2.4 below. However, for the simulations presented here, 5 ripples were assumed across the CATR QZ which is realistic, especially for lower frequency CATR performance. From inspection of these results, it is evident that the amplitude ripple has a greater impact on the resulting far-field "measurements" than was the case for the amplitude taper. Here, the RMS difference level, *i.e.* the RMS value of the magenta trace, was -56.86 dB, -50.68 dB, -44.39 dB and -37.81 dB for the 0.25 dB, 0.5 dB, 1.0 dB and 2.0 dB amplitude peak-to-peak ripple cases respectively with the difference levels increasing towards the boresight direction. Here, even for the 1 dB case, the agreement between the ideal pattern and the simulated measurement is good with the differences being most evident in the change in the level of the nulls depth with smaller differences appearing in the side-lobe levels.

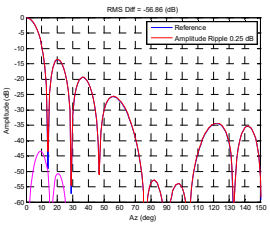

Figure 6: 0.25 dB peak-to-peak amplitude ripple.

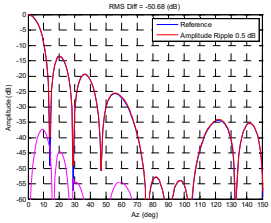

Figure 7: 0.5 dB peak-to-peak amplitude ripple.

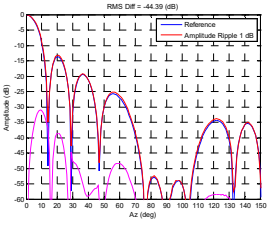

Figure 8: 1.0 dB peak-to-peak amplitude ripple.

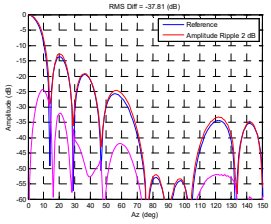

Figure 9: 2.0 dB peak-to-peak amplitude ripple.

2.3 Phase Ripple

The last parameter that was investigated was the phase ripple. Here, the amplitude taper and amplitude ripple was set to zero. Again, the AUT was offset from the origin of the measurement coordinate system by 0.6096 m. The peak-to-peak phase ripple was set to 2.5°, 5.0°, 7.5° and 10.0° and the simulated "measurement" results can be found presented, respectively, in Figures 10, 11, 12 and 13 below.

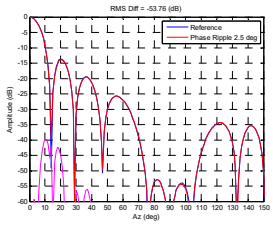

Figure 10: 2.5° peak-to-peak phase ripple.

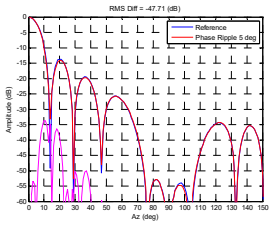

Figure 11: 5.0° peak-to-peak phase ripple.

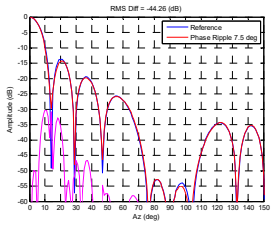

Figure 12: 7.5° peak-to-peak phase ripple.

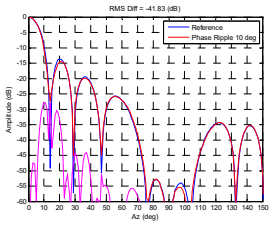

Figure 13: 10.0° peak-to-peak phase ripple.

As before, a spatial frequency of 5 wavelengths across the QZ was used. As before, the amplitude difference level can be seen plotted and is denoted by the magenta trace with the RMS difference level also being computed. Here, the RMS difference level was, respectively, -53.76 dB, -47.71 dB, -44.26 dB and -41.38 dB for the 2.5°, 5.0°, 7.5° and 10.0° peak-to-peak phase ripple cases. As was the case for the amplitude ripple, the greatest differences can be seen in the near-in far-field pattern however, the change in the null depth levels is less pronounced in this case. Otherwise, it is interesting to note that the impact that the phase ripple has on the "measured" far-field patterns is very comparable with the impact that the amplitude ripple has with the 1dB ripple and 10° phase ripple both resulting in RMS difference levels of circa -44 dB an -41 dB respectively. This agrees with theory as a maximum phase error of 10º or a maximum amplitude error of 1 dB could be produced by the same error level [1].

2.4 Ripple Spatial Frequency

Sections 4.2 and 4.3 above considered the effect of amplitude and phase ripple respectively on resulting far-field measurements. However, no consideration was given to the effect of the spectral content of that ripple. In this section the simulations are repeated however in this case the magnitude of the ripple was maintained with the wavelength being varied. Figures 14 and 15 present the far-field amplitude and phase great circle cut for the case of a 1 dB amplitude taper, a 1 dB amplitude ripple and a 10°phase ripple with a spatial frequency of 5, 10, 20, 30 and 40 wavelengths per CATR QZ diameter. The respective plots have been overlaid with the far-field phase patterns being compensated for the physical offset of the AUT in the measurement coordinate system so that the character of the phase patterns is more clearly discernible.

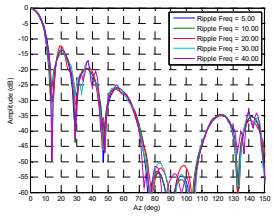

Figure 14: Far-field plot of simulated "measured" amp.

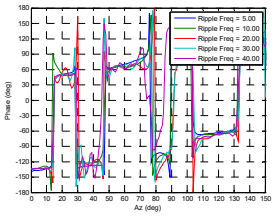

Figure 15: Far-field plot of simulated "measured" phase.

From inspection of Figure 14 it is evident that as the spatial frequency of the ripple increases, the location of the maximum difference between the simulated "measured" pattern and the reference pattern increases in angle with low spatial frequency ripple having a greater effect in the main beam region. For example, the 20 ripple case had the largest impact on the 20° side-lobe. The 5, 10, 20, 30 and 40 ripple cases resulted in a RMS difference level of, respectively, -38.41 dB, -39.82 dB, -40.87 dB, -41.62 dB and -43.23 dB justifying the use of the 5 ripple case considered above as a reasonable worst case upper bound. In practice the amplitude and phase ripple of a real CATR will have a far more complex spectral structure than that considered here. However, the purpose of this work was to establish and verify simple design rules and this is sufficient for that purpose.

2.6 Combined Specification & Position of AUT in CATR

As a final test, the impact of the location of the test antenna within the CATR QZ on the resulting far-field pattern measurements was examined. Here, a 1 dB amplitude taper, 1 dB amplitude ripple and 10° phase ripple was used for the case where the AUT was located at the origin of the measurement coordinate system and again when translated by 0.61 m. Figure 16 shows the amplitude pattern for the case where the AUT was located at the origin of the CATR QZ with 5 ripples while Figure 17 shows the equivalent case only here the AUT had been offset by 61 cm. It is very evident that the RMS difference level has significantly increased as the AUT traverses a larger portion of the QZ. Figures 18 and 19 are equivalent plots only here the case of 10 ripples has been treated with a similar behaviour being evident.

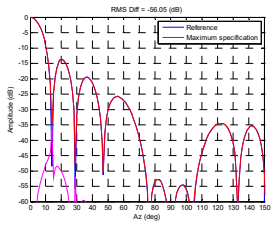

Figure 16: AUT at origin of measurement coordinate system, 5 ripples.

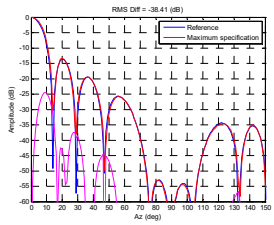

Figure 17: AUT offset from origin of measurement coordinate system by 61 cm, 5 ripples.

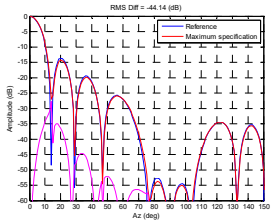

Figure 18: AUT at origin of measurement coordinate system, 10 ripples.

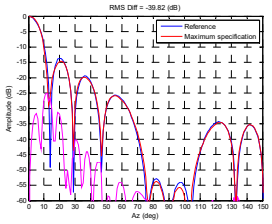

Figure 19: AUT offset from origin of measurement coordinate system by 61 cm, 10 ripples.

For the case where the AUT is offset by 61 cm we find that for the case where we have a 1 dB amplitude taper, 1 dB amplitude ripple and 10° phase ripple obtain a RMS difference level of -39.82 dB (Figure 19). Thus, by using equation (2) above and assuming we wish to know the effect that this would have on a -20 dB side-lobe we can compute this using 20*log10(1 + 10^((-39.82 + 20)/20)) = 0.84 dB. However, for the case where the AUT is offset by 75 cm so that it traverses much of the quiet-zone, *i.e.* 91.8% utilisation, we obtain a higher RMS difference level of -38.98 dB. Here, the effect that this would have on a -20 dB side-lobe would be, *cf.* Equation 2, +20*log10(1 + 10^((-38.98 + 20)/20)) =+0.93 dB and, *cf.* Equation 3, 20*log10(1 - 10^((-39.82 + 20)/20)) =-1.04 dB. This approximates the ±1 dB value which is the accepted rule of thumb that is often stated (never derived from theory) that originates from what one typically sees in practice [7]. We can of course change these values subtly by displacing the AUT by a greater or lesser degree and by adjusting the spatial frequency of the amplitude and phase ripple as has been illustrated above. However, the results obtained above are pretty stable and are sufficient for the purposes of generally specifying a given CATR with the work of [2, 3] being available should actual uncertainties for a known CATR AUT combination be required.

3 Summary and Conclusions

This paper, for the first time, has presented the results of a recent study involving the deployment of a new CATR CEM modelling tool to examining the effect that specific QZ performance parameters have on antenna pattern measurements acquired using a CATR with a pseudo plane wave possessing these properties. It was found that the amplitude ripple and phase ripple parameters are the drivers for the range uncertainty budget with the amplitude taper having a comparatively lesser contribution. It was found that the larger the spatial frequency of the ripple the wider out the maximum effect was observed. Furthermore, it was established that as the AUT was displaced further from the origin of the measurement coordinate system the larger the impact that the amplitude taper amplitude ripple and phase ripple had on the corresponding antenna pattern measurement. This is expected as this implies that the AUT occupies a larger portion of the CATR QZ as it travels larger spatial distances as it is rotated during the course of the measurement. This of course justifies the normal CATR practice of placing the AUT as close to the centre of the QZ as possible as well as aiming to have the AUT rotation axes also at the QZ centre. Finally, it was found that the standard specification for the uniformity of the CATR QZ of having amplitude taper of less than 1 dB, amplitude ripple of less than ±0.5 dB in amplitude and ±5° in phase corresponded to an uncertainty of very nearly ±1 dB on a -20 dB side-lobe level which is in agreement with what one typically sees in practice. This is a very pleasing result as it shows the CATR CEM model agrees with experience and for the first time shows how this uncertainty is comprised.

References

[1] C.G. Parini, S.F. Gregson, J. McCormick, D. Janse van Rensburg “Theory and Practice of Modern Antenna Range Measurements”, IET Press, 2014, ISBN 978-1-84919-560-7.

[2] C.G. Parini, R. Dubrovka, S.F. Gregson, “CATR Quiet Zone Modelling and the Prediction of “Measured” Radiation Pattern Errors: Comparison using a Variety of Electromagnetic Simulation Methods” AMTA October 2015.

[3] C.G. Parini, R. Dubrovka, S.F. Gregson, “Computational Electromagnetic Modelling of Compact Antenna Test Range Quiet Zone Probing: A Comparison of Simulation Techniques”, EuCAP, Davos, Switzerland, April, 2016.

[4] D. Hess; F. Willwerth; R. Johnson, "Compact range improvements and performance at 30 GHz", 1977 Antennas and Propagation Society International Symposium Year: 1977, Volume: 15 Pages: 264 - 267, DOI: 10.1109/APS.1977.1147853

[5] M. Philippakis, C.G. Parini, “Compact antenna range performance evaluation using simulated pattern measurements”, IEE Proceedings Microwaves, Antennas and Propagation, Volume: 143 , Issue: 3 DOI: 10.1049/ip-map:19960398, 1996, Page(s): 200 – 206.

[6] C.G. Parini, M. Philippakis, “The use of quiet zone prediction in the design of compact antenna test ranges”, IEE Proc., Microwave Antennas Propagation, 1996, 143, (3), pp. 193-199.

[7] S.F. Gregson, A.C. Newell, C. Feat, F. Viguier, “The Use of Statistical Image Classification In Assessing Antenna Pattern Measurements”, AMTA October 2013.